Royal knifefish generate powerful suction feeding through large neurocranial elevation and high muscle power output

Ellen Y. Li[1*], Elska B. Kaczmarek[1*], Aaron M. Olsen[1,2], Elizabeth L. Brainerd[1], Ariel L. Camp[3]

[1]Department of Ecology, Evolution and Organismal Biology, Brown University, Providence RI 02912; [2]3D Anatomy Studios, Providence RI; [3]Department of Musculoskeletal and Ageing Science, Institute of Life Course and Medical Sciences, University of Liverpool, Liverpool L7 8TX, UK

*Co-first authors

Running Title:

Royal knifefish generate extreme suction

Key Words:

XROMM, Fluoromicrometry, Muscle strain, Buccal pressure, Body shape, Suction feeding

Summary Statement:

Royal knifefish rely on their distinct postcranial morphology—with a curved vertebral column and large dorsal body muscles—to produce large neurocranial elevation and powerful suction feeding.

ABSTRACT

Suction feeding in ray-finned fishes involves powerful buccal cavity expansion to accelerate water and food into the mouth. Previous XROMM studies in largemouth bass (*Micropterus salmoides*), bluegill sunfish (*Lepomis macrochirus*), and channel catfish (*Ictalurus punctatus*) have shown that more than 90% of suction power in high performance strikes comes from the axial musculature, with cranial muscles primarily acting to transmit power and control cranial kinematics. Royal knifefish (*Chitala blanci*) have an unusual hump-like appearance, a product of a curved vertebral column and a large mass of epaxial muscle. Based on their body shape, we hypothesized that royal knifefish would generate high power strikes by utilizing large neurocranial elevation, vertebral column extension, and epaxial shortening. As predicted, *C. blanci* generated high suction expansion power compared to the other three species studied to date (up to 160 W), which was achieved by increasing both the rate of volume change and the intraoral subambient pressure. Such increases are likely a product of its large epaxial muscle (25% of body mass) shortening at high velocities to produce large neurocranial elevation (18-28 deg) and vertebral flexion, as well as high muscle mass-specific power (up to 800 W kg^{-1}). For the highest power strikes, axial muscles generated 99% of the power, and 60% of the axial muscle mass consisted of the epaxial muscles. This supports our hypothesis that postcranial morphology may be a strong predictor of suction feeding biomechanics.

INTRODUCTION

High performance suction feeding in ray-finned fishes is both fast and forceful, thus requiring high power to expand the buccal cavity and suck in prey. Instantaneous suction expansion power can now be measured empirically by using X-ray Reconstruction of Moving Morphology (XROMM) to measure instantaneous buccal cavity volume and subsequently the instantaneous rate of buccal cavity expansion (Camp et al., 2015). Combined with measurements of subambient buccal pressure, buccal volume measurements make it possible to calculate instantaneous suction expansion power as the product of rate of buccal volume change and subambient buccal pressure (Van Wassenbergh et al., 2015).

To date, suction expansion power has been measured with XROMM in three species of ray-finned fishes: largemouth bass (*Micropterus salmoides*), bluegill sunfish (*Lepomis macrochirus*), and channel catfish (*Ictalurus punctatus*) (Camp et al., 2015; Camp et al., 2018; Camp et al. 2020). In the highest performance strikes from all three species, the empirically measured suction power was far too great to have been generated by muscles in the head region alone. Instead, more than 90% of suction power came from epaxial and hypaxial musculature (largemouth bass and bluegill sunfish) or the hypaxial musculature (channel catfish). Furthermore, the axial musculature was found to actively shorten along 60-70% of the length of the body, encompassing the vast majority of the axial muscle mass (Camp et al., 2015; Camp et al., 2018; Camp et al., 2020; Jimenez and Brainerd, 2020; Jimenez and Brainerd, in press). Thus, although it has long been known that axial musculature contributes to suction feeding (Liem, 1967; Osse, 1969), the ability to measure suction power, muscle length, and activation has revealed that some fish use nearly their whole bodies for suction feeding. The overall body shape and musculoskeletal morphology should therefore be taken into account when studying the biomechanics and energetics of suction feeding.

Axial muscle mass, distribution, and insertions onto the neurocranium and pectoral girdle are likely important for the generation of suction power and the transmission of power to the head (Carroll et al., 2004; Collar and Wainwright, 2006). For example, muscle mass distribution is a key concept in Carroll's "morphological potential" of suction feeding (Carroll et al., 2004). Largemouth bass have a fusiform body shape, while bluegill sunfish have deeper bodies and have more bony processes (i.e. supraneurals, neural spines, and pterygiophores) immediately caudal to the neurocranium. Jimenez et al. (2018) found that fish with deeper bodies and with more bones occupying the region immediately caudal to the neurocranium produce less

neurocranial elevation. Consistent with those results, XROMM suction feeding studies also found that bluegill sunfish produced less neurocranial elevation than largemouth bass (Table S1) (Camp and Brainerd, 2014; Camp et al., 2018). In addition, channel catfish often produced little to no neurocranial elevation (Table S1) (Camp et al., 2020). While channel catfish are not deep bodied, they have many bones caudal to the neurocranium that inhibit neurocranial elevation, including broad bony struts (nuchal plates) connecting the neurocranium to the dorsal spine, large dorsal pterygiophores, and cranial vertebrae modified for hearing (Weberian apparatus). Channel catfish also have a robust pectoral girdle that supports the pectoral spine and has a broad attachment area for the massive hypaxials. Channel catfish rely solely on the hypaxials to generate suction power, and yet their suction strikes were similar in power to those of largemouth bass and bluegill sunfish (Camp et al., 2020). The distribution of epaxial muscle near its attachment to the neurocranium is also informative about the biomechanics of suction feeding. While bluegill sunfish and largemouth bass produced similarly powered strikes, bluegill sunfish generated much greater subambient buccal pressures than largemouth bass (Table S1) (Camp et al., 2015; Camp et al., 2018; Carroll et al., 2004). Biomechanical modeling of force transmission has demonstrated that the larger epaxial cross-sectional area and longer epaxial moment arms (for neurocranial elevation) of bluegill sunfish, relative to largemouth bass, contribute to the greater subambient pressures that bluegill sunfish are capable of generating (Carroll et al. 2004). Therefore, examining inter-species differences in postcranial musculoskeletal morphology enhances our understanding of suction feeding biomechanics. But only a small sample of body shapes has been investigated so far, and none of the previously studied species predominantly use the epaxial muscles to generate suction power.

Royal knifefish (*chitala blanci*) offer an interesting model for studying suction feeding, as they are both morphologically and phylogenetically distinct from species previously studied with XROMM. The royal knifefish is a member of the family Notopteridae (order Osteoglossiformes) and is not closely related to the orders Siluriformes (which contains channel catfish) nor Centrarchiformes (which contains largemouth bass and bluegill sunfish). Morphologically, royal knifefish appear to have a hump-like shape caudal to the neurocranium, dorsoventrally “tall” epaxial musculature, laterally compressed body, and an inverted teardrop shaped cross-section. These features create an exaggerated body shape that is distinct from those previously studied with XROMM. One unusual feature of royal knifefish is their hump-like

appearance just caudal to neurocranium. Based on previously published images (X-ray images and frames from high-speed videos) of clown knifefish (*Chitala ornata*), we suspected that the hump-like appearance was both a product of a curved vertebral column and a large mass of epaxial muscle (Coombs and Popper, 1982; Sanford and Lauder, 1989). In addition, the body shape of royal knifefish is very laterally compressed and has an inverted teardrop shape when viewed from a transverse cross-section, with the epaxial muscles being the thickest portion of the body and tapering in thickness ventrally towards the hypaxials and anal fin (Fig. 1B). It is worth noting that the royal knifefish is not closely related to Neotropical knifefishes in the order Gymnotiformes, the two groups having independently evolved similar body forms (Betancur-R et al., 2017). However, at least one species of gymnotid knifefish generates extremely fast fluid flows and large subambient pressures during suction feeding--sufficient to induce cavitation (Ortega-Jimenez and Sanford, 2020)--hinting that this body shape may be linked to powerful suction feeding.

Of the species previously studied with XROMM, bluegill sunfish have the most similar body shape to royal knifefish. Both royal knifefish and bluegill sunfish have laterally compressed bodies, curved vertebral columns, and dorsoventrally “tall” epaxial muscles. In bluegill sunfish, the epaxial muscles have a longer moment arm for neurocranial elevation and larger cross-sectional area compared to largemouth bass, and these features enable bluegill sunfish to generate greater subambient buccal pressure (Carroll et al. 2004). In royal knifefish, its hump-like appearance seems to be the result not just of a curved vertebral column, but also of localized hypertrophy of the epaxial musculature. This suggests that the epaxial muscle of royal knifefish may have a large cross-sectional area and large moment arm, similar to bluegill sunfish, which may enable them to generate similarly low buccal pressures. Of the species previously studied, bluegill sunfish generated the most powerful suction expansion relative to their body and muscle mass, by generating higher subambient buccal pressures with smaller axial muscles. Since royal knifefish seem to have similar epaxial morphology, we suspect that royal knifefish should also be able to generate high suction powers, relative to their muscle mass.

While royal knifefish and bluegill sunfish have similar morphological features, royal knifefish differ from bluegill sunfish in key ways, which we hypothesize will result in much higher neurocranial elevation and epaxial contribution in royal knifefish. Royal knifefish have a head and body that are more laterally compressed and elongated, a more ventrally flexed

vertebral column, fewer bony processes caudal to the neurocranium, and a far greater proportion of epaxial muscle than bluegill sunfish. While the vertebral column of bluegill sunfish is slightly curved, the vertebral column of royal knifefish has a more exaggerated curvature. Its ventrally flexed shape causes the neurocranium to have a depressed resting posture, which we expect increases the range of motion of the neurocranium. Additionally, the curvature may also cause the axis of rotation of the neurocranium to be located more caudally (closer to the vertebral column inflection point), which has also been correlated with greater neurocranial elevation in suction feeding fishes (Jimenez et al., 2018). Therefore, we predict that royal knifefish are capable of higher neurocranial elevation than bluegill sunfish. Another important difference between royal knifefish and bluegill sunfish is that while bluegill sunfish have many bony processes immediately caudal to the neurocranium, knifefish have few bones in this region (no supraneural bones or dorsal fin pterygiophores, and thin neural spines). Deep bodied fish with more bones in this region, like sunfish, produce less neurocranial elevation (Jimenez et al. 2018), which is consistent with XROMM kinematic data (Table S1) (Camp and Brainerd, 2014; Camp et al., 2018). Because royal knifefish have very few bones in this region, and we predict that this also enables them to perform larger neurocranial elevation than bluegill sunfish. Lastly, while both royal knifefish and bluegill sunfish have "tall" epaxial muscles, the inverted teardrop shape of the royal knifefish (when viewed in transverse cross-section) increases the proportion of epaxial muscles mass relative to the rest of the body, thereby increasing muscle power. Based on the body shape of the royal knifefish, we hypothesized that the royal knifefish generates larger neurocranial elevation and has a greater epaxial muscle mass relative to bluegill sunfish (Camp et al., 2018). If all other aspects of suction expansion are similar in knifefish and sunfish, this greater neurocranial elevation should result in greater mouth expansion and ultimately suction power.

To test these hypotheses, we used XROMM to measure 3D skeletal kinematics of royal knifefish during suction feeding. These 3D XROMM animations were used to measure the magnitude of cranial elevation, as well as the instantaneous volume of the buccal cavity using a dynamic digital endocast (Camp et al., 2015; Camp et al., 2020). Intraoral pressure was also measured simultaneously and combined with the rate of volume change to calculate the suction expansion power during knifefish strikes. Length changes were measured throughout the epaxial, hypaxial, and sternohyoid muscles during suction feeding with fluoromicrometry (Camp et al.,

2016). Muscle shortening and post-mortem muscle mass were used to determine the roles and relative contributions of these muscles to suction power. These data allowed us to compare suction feeding in royal knifefish to previously studied species (bass, sunfish and catfish) and test if knifefish have 1) relatively large cranial elevation and epaxial muscle mass, 2) relatively powerful suction expansion. Determining how knifefish use their unique postcranial morphology to power suction expansion provides a better understanding of the relationship between body shape and suction feeding biomechanics.

MATERIALS AND METHODS

Three royal knifefish (*Chitala blanci*, d'Aubenton 1965) were acquired from Ocean State Aquatics, Coventry RI: Cb01 (standard length 35.6 cm, body mass 217 g), Cb03 (standard length 30.8 cm, body mass 170 g), and Cb04 (standard length 43.3 cm, body mass 480 g). Royal knifefish were maintained on a diet of goldfish (*Carassius auratus*). All experimental procedures were approved by Brown University Institutional Animal Care and Use Committee.

Each fish was anesthetized with a buffered MS-222 solution during surgical implantation of a buccal cannula for pressure measurement and radio-opaque bone and muscle markers. Implantation techniques were consistent with those previously reported (Camp and Brainerd, 2014), and are described here in brief. One to five radio-opaque markers (tantalum spheres 0.50 or 0.80 mm in diameter) were implanted into the neurocranium, the left and right ceratohyals and cleithra, and the left maxilla, lower jaw, suspensorium, and operculum (Fig. 2. A,B). Cb04 received bilateral lower jaw implantations. In all individuals, 0.80 mm tantalum beads were implanted superficially to the left of the mid-sagittal plane in the epaxial (five to nine markers), and sternohyoid musculature (two to three markers) (Fig. S1). Ventral muscles were marked in Cb01 (anal fin) and Cb04 (hypaxial) with three to five markers, with no ventral markers in Cb03. The dorsal column of epaxial musculature was implanted in Cb04 (three markers) (Fig. S1). Four to six markers implanted in the axial muscles were used to define a body plane (Fig. S1). Following established methods, a cannula guide for the pressure transducer was implanted into the ethmo-frontal region of the neurocranium, avoiding the palatine and teeth, protruding just into the buccal cavity (Norton and Brainerd, 1993). All individuals received postoperative analgesic (butorphanol) and an antibiotic (enrofloxacin) and fully recovered aggressive feeding

behaviors within three days; no signs of distress or difficulty caused by any of the implants were observed.

Data recording

All fish were trained to feed on live goldfish (approximately 3-5 cm) in custom-built acrylic aquaria with a feeding extension tunnel (75–100 mm wide, 300-400 mm long) designed to minimize the amount of water through which the X-ray beams must travel (Gidmark et al., 2012).

A custom biplanar X-ray system (Imaging Systems and Services, Painesville, OH, USA) was used to capture dorsoventral and lateral X-ray videos at 500 frames s^{-1} with Phantom v10 high-speed cameras (Vision Research, Wayne, NJ, USA) at 100 mA and 90-115 kV. Standard grid and calibration objects were used to remove distortion introduced by X-ray machines and to calibrate three-dimensional (3D) space (Brainerd et al. 2010). Intraoral pressure was simultaneously recorded with an SPR- 407 Mikro-tip pressure probe (Millar Instruments, Houston, TX, USA) inserted into the neurocranial cannula, recording at 1000 Hz with PowerLab and LabChart 7.2.2 (ADInstruments, Colorado Springs, CO, USA). Pressure transducer calibration was carried out daily. Pressure data were collected for each strike and noise was filtered in R (2019, R Core Team, Vienna, Austria) using a low-pass Butterworth filter with a 60 Hz cutoff. The pressure recording was initiated by the X-ray camera trigger with a mean lag of two milliseconds (range 1-3 ms) from the initial X-ray image. For three Cb03 strikes, the initial X-ray images were missing, so to correctly align the pressure and video data, we averaged the time between peak pressure and peak rate of volume change for all Cb04 strikes and corrected the Cb03 image sequences to account for a pressure lag of two milliseconds. Feeding trials with the greatest subambient buccal pressure from each individual were chosen for analysis. A total of 23 recorded strikes (six from Cb01, seven from Cb03, ten from Cb04) were analyzed.

Computed tomography (CT) scans were taken of each fish after surgical implantation with a FIDEX CT Scanner (Animage, Pleasanton, CA, USA), with 480 × 480 pixel resolution and 0.173 mm slice thickness. From these scans, polygonal meshes of each bone and the radio-opaque markers were generated in Horos (v3.3.5; Horos Project; horosproject.org) and edited in Geomagic 2014 (Research Triangle Park, NC, USA). Markers were imported into Autodesk Maya 2020 (San Rafael, CA, USA) and with custom scripts from 'XROMM Maya Tools'

package--available at https://bitbucket.org/xromm/xmalab--their respective *xyz* (3D) coordinates were determined. Raw data for this study are publicly available and stored on the XMAPortal (http://xmaportal.org) in the study "Knifefish Suction Feeding," with the permanent identifier BROWN65. Video data are stored with their essential metadata in accordance with best practices for video data management in organismal biology (Brainerd et al., 2017).

XROMM animation

For each of the three individual *C. blanci*, skeletal kinematics were reconstructed using marker-based XROMM with XMALab 1.5.5 (Knörlein et al., 2016; software and instructions available at https://bitbucket.org/xromm/xmalab) and custom XROMM MayaTools scripts (available at https://bitbucket.org/xromm/xromm_mayatools). Markers from both X-ray videos were tracked in XMALab with a mean precision of 0.004 cm and maximum precision error of 0.01 cm across all trials and were used to determine the *xyz* coordinates across all markers and individuals. These marker coordinates were used to reconstruct the 3D motion of each bone using the 'matools' R package, following the XROMM workflow described in Olsen et al., 2019 (available under matools R package at https://github.com/aaronolsen). Briefly, all *xyz* marker coordinates were smoothed and, for bones containing three or more markers, 3D coordinates were combined with their respective CT coordinates (using the 'unifyMotion' function from 'matools') to produce rigid body transformations. These transformations were applied to the skeletal bone meshes in Maya (2020, Autodesk), producing a 3D XROMM animation of each suction feeding strike (Fig. 2A,B). For any bones with only two beads or those with a linear set of markers, virtual constraints were applied using the 'matools' R package in accordance with anatomical constraints (e.g. cartilaginous fusion between the cranioventral region of the left and right cleithra, or ceratohyal retraction along the neurocranial midsagittal plane).

The body plane was animated with a set of 5 intramuscular axial markers in roughly the same location along the body for each individual. These markers were positioned near the most curved region of the vertebral column. Their 3D coordinates were combined with their respective CT coordinates to generate a rigid body transformation using the 'matools' R package (Olsen et al., 2019). The body plane animation was included in the XROMM animations mentioned above.

Skeletal kinematics

Six-degree-of-freedom motions of the neurocranium and left cleithrum were measured relative to the body plane. Following previously established methods, these rotations were measured by using a joint coordinate system (JCS), which measures the relative rotations of two anatomical coordinate systems (ACSs), one attached to the bone and the other to the body plane (Camp and Brainerd, 2014; Camp et al., 2018). Each JCS measured translation and Euler angle rotations about the x-, y-, z- axis, following the right-hand rule and *zyx* order of rotation. The JCS used to measure neurocranial motion was placed at the craniovertebral joint and the JCS to measure cleithral motion was placed at the dorsal tip of the cleithra. Both sets of JCSs were aligned with the z-axis oriented mediolaterally, y-axis rostrocaudally, and the x-axis dorsoventrally. Positive rotation about the z-axis reflects dorsal rotation in the sagittal plane, corresponding to neurocranial elevation or cleithral protraction. Rotations about the z-axis also capture motions of the cranial vertebrae.

Dynamic endocast

Following previously established methods, changes in buccal cavity volume were measured from XROMM animations using a dynamic endocast (Camp et al., 2015; Camp et al., 2020). In brief, a polygonal mesh endocast of the left side of the buccal cavity was generated using locators attached to the inside surface of cranial bones. Additional locators were placed between bones to define the ventral border of the buccal cavity, i.e., the sternohyoid and protractor hyoideus muscles, and the mid-sagittal plane dividing the left and right sides of the buccal cavity. The 3D coordinates of the locators were imported into MATLAB (R2020a; MathWorks, Natick, MA, USA) and custom-written scripts (available at https://bitbucket.org/ArielCamp/dynamicendocast) were used to generate the volume enclosing the locators and calculate its volume, for each frame. The volumes were generated using the 'alphashape' function in MATLAB with an alpha value of 3, and polygonal obj meshes of the volumes of the left side of the buccal cavity were then imported into Maya for visual verification (Fig. 2E,F). Under assumptions of bilateral cranial symmetry, the left mesh volume was doubled to approximate bilateral buccal volume expansion.

Muscle length changes

Sternohyoid and axial muscle length changes were measured from X-ray videos as the vector-distance between intramuscular markers, i.e., by fluoromicrometry (Camp et al., 2016). Muscle markers were tracked in XMALab and their coordinates were filtered in R with 'matools' as described above. The distance between muscle markers was subsequently calculated in R to determine the magnitude and distribution of sternohyoid, epaxial, and hypaxial muscle shortening. To capture muscle shortening in the cranialmost region of the epaxial muscle and the dorsal column of Cb04, the distance was measured between the first marker in the muscle region and a locator placed at the cranialmost neurocranium-epaxial muscle attachment site in Maya. Distance in the cranialmost hypaxial region was calculated between the first hypaxial muscle marker and a locator attached to the cleithra, placed in line with the hypaxial muscle bead set (Fig. S1). Since the entire marker set was not consistently within the X-ray imaging volume, axial muscle length was measured from a subset of axial muscle markers that were visible in almost all strikes. This set of markers extended approximately 7-9 cm caudal of the craniovertebral joint: from the neurocranium to as far back as a few centimeters cranial of the dorsal fin (Fig. S1). Within this region, fluoromicrometry was used to estimate the muscle lengths of subregions along the length of the body by measuring distance between adjacent pairs of intramuscular markers.

Whole-muscle length was calculated by taking the sum of the subregional muscle lengths, originating with the cranialmost locator and extending to the caudalmost visible muscle marker. In the sternohyoid, all implanted markers were visible, and its measurements are reported as whole-muscle length. Muscle length at each time step was normalized by the mean initial length measured at the first recorded frame of each strike (L_i), with values less than 1 representing that the muscle had shortened. Muscle velocity was similarly calculated at each time as the change in normalized muscle length divided by the change in time, denoted by L_i s^{-1}, with positive values representing muscle shortening. Note that this method for determining axial muscle strain differs slightly from other suction power studies, in that we used the sum of the subregional muscle lengths, whereas prior papers used the distance from the neurocranium or cleithrum to the caudalmost axial muscle marker (Camp et al., 2015; Camp et al., 2018; Camp et al., 2020). The summation method recorded more consistent levels of epaxial muscle shortening in *C. blanci*, likely due to its ability to capture the length of the naturally curved epaxial musculature at rest.

Power calculations

Estimations of instantaneous suction expansion power were calculated in R as the product of rate of volume change ($m^3 s^{-1}$) and intraoral pressure (Pa) as described in Camp et al (2015). Before calculating rate of volume change, bilateral buccal volume estimates from the dynamic endocast were filtered with a low-pass Butterworth filter (150 Hz cutoff) to reduce noise generated by frame-to-frame polygonal mesh re-triangulations. Buccal pressure was downsampled from 1000 Hz to 500 Hz to match the frequency of the volume data. Pressure data were calculated relative to initial, ambient pressure prior to the strike and multiplied by -1, so that at each time step, the product of subambient pressure and increasing rates of volume change would reflect positive power (Fig. 3).

For each strike, axial and cranial mass-specific power were calculated by dividing the maximum instantaneous power by the mass of the respective muscle types. Muscle masses were determined by post-mortem dissection of the muscle regions on the right side of the fish, weighed on a digital scale, and then doubled to estimate bilateral muscle mass for all individuals except Cb03. The body of Cb03 was unavailable for dissection, so muscle masses are estimates determined by averaging the percent of muscle mass for each muscle of Cb01, Cb04, and an additional individual, Cb02, and assuming proportionality based on overall body mass across individuals (Table 1). The total body mass, and bilateral epaxial, hypaxial, dorsal column, sternohyoid, and cranial muscle masses from Cb02 were 0.393 kg, 0.103 kg, 0.066 kg, 0.002 kg, 0.0032 kg, and 0.0054 kg respectively (values for other individuals are reported in Table 1). Axial mass-specific power was calculated by dividing instantaneous power by the sum of the epaxial, hypaxial, and dorsal column muscle mass extending approximately three centimeters caudal to the dorsal fin. Cranial mass-specific power was calculated by dividing instantaneous power by the combined mass of the levator arcus palatini, dilator operculi, levator operculi, and sternohyoid muscle. Muscle mass-specific power was determined by dividing the maximum instantaneous power by the total mass of the muscle regions (epaxial, hypaxial, and sternohyoid muscle) shortening during suction expansion (Fig. 3). These mass-specific values represent the estimated amount of power each group of muscles would need to output if they were the sole contributors to suction feeding expansion.

The volume calculations and pressure data do introduce sources of error in the suction power estimates, as described in Camp et al. (2018). In brief, absolute volume measurements are overestimates, since they do not account for the presence of soft tissue or internal structures. However, these structures are present throughout the strike and should have little effect on the calculations for rate of volume change and subsequent power calculations. Rapid re-triangulation of dynamic endocast polygonal meshes may cause increased recorded rates of volume change, however, a low-pass Butterworth filter with a high cutoff frequency over the endocast buccal volume trace may produce underestimates of the actual rate of volume change. The intraoral pressure cannula only provides pressure readings at one location within the buccal cavity and does not capture variations in pressure during suction feeding (Muller et al., 1982; Van Wassenbergh, 2015). These estimates are likely underestimates of subambient pressure, since modeling of clariid catfishes and bluegill sunfish (Van Wassenbergh et al., 2015) and *in vivo* measurements (Tegge et al., 2020) suggested that highest subambient pressure occurred more caudally in the buccal cavity (Van Wassenbergh et al., 2005; Van Wassenbergh et al., 2006). Additionally, our power calculations do not account for the forces required to overcome inertia or drag (Van Wassenbergh et al., 2015), yet studies of clariid catfishes and largemouth bass indicate that these forces are likely small compared to that required to overcome subambient forces (Van Wassenbergh et al., 2005; Van Wassenbergh et al., 2015). Therefore, our values for instantaneous suction power may be underestimates.

Determining peak gape

Suction feeding power, muscle shortening, and skeletal kinematics were all measured relative to the time of peak gape. Gape distance was measured as the vector-distance between virtual locators on the rostralmost tips of the lower jaw and neurocranium. Peak gape is defined here as the initial maximum gape distance directly following the rapid increase in gape during the start of the strike. We calculated this by identifying the first frame at which there is a major change in the inflection of the gape distance curve from increasing to decreasing or in some cases minimal increasing. By taking the derivative of gape distance over time, we used 10% of the maximum rate of gape change as a threshold to isolate the first time point when the rate of gape change was below the threshold. This method for determining peak gape differs from other suction power studies (Camp et al., 2015; Camp et al., 2018; Camp et al., 2020), but was chosen

because of the high variability of gape distance traces in royal knifefish, e.g., gape curves with multiple peaks (double-strikes) or initial strikes followed by slow gradual gape expansion (slowly increasing plateau). Selecting the initial peak gape frame using the first instance of major inflection in gape distance yielded substantially better consistency of alignment of the expansion part of the gape cycle in this study (Fig. S2).

RESULTS

Two out of three of the royal knifefish in our study generated exceptionally high suction power (Fig. 4). The neurocranium reached high magnitudes of elevation and consistently reached peak elevation during the period of peak suction power (Fig. 5). Similarly, the epaxial muscle generated high strain and shortening velocity, reaching its shortest length during the period of peak power, and the sternohyoid shortened consistently across all strikes (Fig. 5). In addition, muscle mass-specific power was exceptionally high, nearing the expected limits of muscle power generation in vertebrates (Fig. 4).

Inter-individual variation

Cb04 produced substantially higher power strikes than Cb01 and Cb03 (Fig. 4). The mean peak power for Cb04 was nearly 16 times greater than Cb01 and 7 times greater than Cb03 with their most powerful strikes reaching 12.9 W for Cb01, 33.7 W for Cb03, and 161.6 W for Cb04. The substantially larger suction expansion power in Cb04 was explained by the combination of both greater subambient buccal pressure and faster rate of buccal volume change (Table 1). Mean peak subambient pressure in Cb04 was approximately 5.5 times greater than that of Cb01 and 3 times greater than that of Cb03 (Table 1). The mean peak rate of volume change was 3 times greater than Cb01 and Cb03. Unlike Cb04, the difference in suction expansion power between Cb01 and Cb03 was largely due to the difference in mean peak subambient buccal pressure. While the mean peak rate of buccal volume increase was similar between Cb01 and Cb03 (835 ± 51 cm^3 s^{-1} and 829 ± 67 cm^3 s^{-1}, respectively; mean ± s.e.m.), the mean peak subambient buccal pressure was nearly two times larger in Cb03 compared to Cb01 (-7.8 ± 0.8 kPa and -14.9 ± 1.7 kPa, respectively). Because of these differences among individuals, results are reported separately for each individual, with means and s.e.m. (Table 1).

412 **Skeletal kinematics**

413 The neurocranium and cranialmost vertebrae consistently elevated (rotated dorsally)
414 relative to the body plane, across all strikes in all individuals (Fig. 5). During suction expansion,
415 as the vertebral column extended from rounded to straight, the cranialmost vertebrae elevated
416 with the neurocranium (Fig. 2A,B). Due to placement of our body plane, the neurocranium JCS
417 captures a combination of neurocranium elevation at the craniovertebral joint and vertebral
418 column extension. The mean maximum elevation measured during peak power was 18.1 ± 1.1
419 deg for Cb01, 26.5 ± 2.1 deg for Cb03, and 27.8 ± 0.5 deg for Cb04. For some strikes, the
420 neurocranium showed a pattern of initial elevation, slight depression, and then continued
421 elevation at the end of pectoral girdle retraction. The initial phase of neurocranial elevation
422 occurred during the period of maximum suction expansion power (shown in red in Fig. 5) and
423 during epaxial muscle shortening (Fig. 5).

424 Cleithral retraction (caudoventral rotation) relative to the body plane was consistent
425 within Cb04 strikes, but highly variable in Cb01 and Cb03 (Fig. 5). Cb04 strikes showed a
426 consistent pattern of initial cleithral protraction (craniodorsal rotation), followed by the start of
427 retraction prior to maximum suction expansion power, and a steady, continued retraction through
428 the period of peak expansion power (Fig. 5). It should be noted that cleithral protraction occurs
429 relative to the body plane; the cleithra are not protracting relative to the neurocranium but are
430 instead being pulled dorsally by vertebral column extension, causing hypaxial lengthening.
431 Maximum cleithrum retraction in Cb04 averaged -3.3 ± 0.3 deg during the period of maximum
432 expansion power and increased to an average of -6.4 ± 0.2 deg after peak power. Cb01 and Cb03
433 showed variability in timing and did not always retract during the period of peak power in their
434 strikes. The magnitude of cleithral protraction and retraction was also highly variable in Cb01
435 and Cb03 (Fig. 5), with mean maximum retractions of -3.5 ± 1.2 deg and 0.6 ± 1.2 deg,
436 respectively, during the period of peak power.

437

438 **Muscle length changes and muscle power**

439 The epaxial and sternohyoid muscles consistently shortened prior to and during peak
440 power in all individuals (Fig. 5). However, the magnitude and pattern of epaxial shortening
441 varied across individuals. Epaxial muscles shortened across all the measured subregions in Cb03
442 and Cb04, and all but the last subregion of Cb01 (Fig. 6). Mean peak whole-muscle strain in the

epaxials during peak power was similar between Cb04 and Cb03 (7.9 ± 0.2 % L_i and 7.6 ± 0.7% L_i, respectively). Mean peak muscle shortening velocity was higher in Cb04 (4.1 ± 0.1 L_i s^{-1}) than in Cb03 (3.2 ± 0.5 L_i s^{-1}). Epaxial strains were lower in Cb01, approximately half that of Cb03 and Cb04 (Table 1). Mean maximum epaxial strain during peak power was lowest in the cranialmost region (below 5% strain in all individuals) and the highest at approximately one-half to three-fourths of the distance between the craniovertebral joint to the dorsal fin (3-6 cm, 4-7 cm, and 6-8 cm caudal of the craniovertebral joint in Cb01, Cb03, and Cb04, respectively) (Fig. 6; Fig. S1).

Similar shortening behaviors were seen in the dorsal column of muscle of Cb04, the only individual with beads implanted in this muscle (Fig. S3). This column of muscle is dorsal to and separate from the epaxial. It inserts on the neurocranium and extends along the length of the body. The dorsal column of Cb04 shortened at the same time as the corresponding region of the epaxial muscle (three cranialmost subregions), reaching 5.6 ± 0.1% L_i strain and muscle shortening velocity of 3.2 ± 0.1% L_i (Fig. S3). The caudalmost subregion also showed the greatest magnitude of strain.

In the hypaxial musculature of Cb04, a consistent pattern of lengthening then shortening prior to the period of peak power occurred in all of its recorded strikes (Fig. 5). Early lengthening across the full extent of the marked hypaxial muscle was so great in Cb04 that during peak power it shortened with a mean peak velocity of 3.8 ± 0.1 L_i s^{-1}, while the muscle length was still longer relative to its initial length (-1.5 ± 0.4 % L_i strain) (Table 1). The caudalmost subregion of the hypaxial muscle shortened during the period of peak power, while the cranialmost subregions lengthened (Fig. 6). Unlike Cb04, ventral muscle beads in Cb01 were implanted in the anal fin musculature, and no beads were implanted in the hypaxial muscle of Cb01 or Cb03 (Fig. S1). The shortening patterns and strain of the ventral muscle beads in Cb01 were highly variable (2.7 ± 1.3% L_i) (Fig. 5, Table 1).

The sternohyoid shortened with a consistent pattern in all strikes and across individuals, with mean strains of 2.3-3% during the period of peak power (Table 1, Fig. 5). Sternohyoid shortening began prior to and continued through the period of peak power, with higher shortening velocities occurring during peak power. Magnitudes of strain in the sternohyoid were similar across individuals, but sternohyoid shortening velocity was highest in Cb04 (4.6 ± 0.2 L_i s^{-1}) compared to Cb01 and Cb03 (2.8 ± 0.3 L_i s^{-1} and 2.3 ± 0.4 L_i s^{-1}, respectively) (Table 1).

Unlike the epaxial musculature, where Cb03 had higher strain and muscle shortening velocities than Cb01, higher sternohyoid strain and muscle shortening velocities occurred in Cb01 (Table 1).

Royal knifefish generated high muscle mass-specific power, which we calculated by dividing the maximum instantaneous suction power of each strike by the total mass of musculature shortening during peak power generation (epaxial, hypaxial and sternohyoid). For these muscles alone (0.2035 kg combined for Cb04) to produce the highest power strike recorded (161.6 W), Cb04 would have needed to generate 794.1 W kg^{-1} of muscle power. The next three highest power strikes recorded for Cb04 are estimated to have required 628.0 W kg^{-1}, 623.1 W kg^{-1}, and 614.2 W kg^{-1}. The maximum peak muscle power in Cb04 was much greater than that of the highest power strike in Cb01 (156.9 W kg^{-1}), but the muscle power in the highest power strike in Cb03 (474.0 W kg^{-1}) was within the range of muscle power generated across all Cb04 trials (287.1 W kg^{-1} - 794.1 W kg^{-1}) (Table 1).

DISCUSSION

Royal knifefish generated much greater suction power than was observed in largemouth bass (Camp et al., 2015), bluegill sunfish (Camp et al., 2018), and channel catfish (Camp et al., 2020) by producing both greater subambient intraoral pressure and a greater rate of buccal expansion. The massive epaxial muscles (25% of body mass) shortened considerably and with a high shortening velocity. Epaxial shortening generated substantial neurocranial elevation and vertebral column extension. These results agree with our predictions based on the body shape and craniovertebral morphology. During the most powerful strikes, the hypaxials also shortened markedly and together with the epaxials generated over 99% of the power for suction expansion--requiring muscle power outputs of up to nearly 800 W kg^{-1}. The sternohyoid muscle shortened consistently in all strikes to generate power, while axial muscle shortening was more variable during lower power strikes. This suggests that the sternohyoid muscle may contribute a greater proportion of power in lower power strikes.

Variation in suction power

Knifefish are capable of generating very high suction power, but we observed a wide range of power across the three individuals. Cb04 produced substantially higher power strikes,

with the mean peak suction power values nearly ten times greater than that of Cb01 and six times that of Cb03 (Fig. 4). Suction power is calculated by multiplying the rate of buccal cavity volume change by the intraoral pressure. Cb04 generated more power than the other individuals by both increasing its rate of buccal volume change and intraoral pressure. The higher performance of Cb04 is in part explained by its larger mass. The total body mass of Cb04 was more than twice as high as those of Cb01 and Cb03 (Table 1), providing more muscle mass to generate power with. However, body size cannot completely explain intraspecific variation in power, as Cb03 has the smallest total body mass (78% of that of Cb01), and yet it generated the same mean rate of buccal volume change as Cb01, and even greater mean magnitude of buccal pressure (Table 1). Notably, the highest power Cb03 strike was more than double that of Cb01 (Fig. 4). Motivation almost certainly contributed to this variation as well. Despite efforts to standardize prey type, prey size, and training, Cb04 responded better to training, was less timid when feeding in front of researchers, and was highly food motivated. The top three Cb03 strikes required roughly the same amount of mass-specific muscle power as the three lowest Cb04 strikes, suggesting that Cb04 may not be merely an exceptional individual, but instead a good representation of the capabilities of highly motivated royal knifefish.

The variation between knifefish individuals is similar to what has been observed in bluegill sunfish, largemouth bass, and channel catfish. In all these species the highest performing individual generated muscle mass-specific suction power that was at least 2.0 times higher than the second highest performing individual (Camp et al., 2015; Camp et al., 2018; Camp et al., 2020). And a wide range of maximum suction power, intraoral pressure, and buccal volume change was observed, even when accounting for body or mouth size. Both the present study of knifefish and previous suction power studies are unlikely to have captured the maximum performance of any of these species, given the difficulty of capturing maximum performance in lab-based studies with artificial environments and small sample sizes (Astley et al., 2013). Therefore, even the highest power strikes, such as those of Cb04, are conservative estimates of the suction power capacity of these species. Without having captured the true maximums of each species, conclusions from interspecies comparisons can only be drawn from the data that has been collected from each species. Thus while knifefish suction expansion appears impressively powerful compared to previously measured species, it is difficult to directly compare suction power across species.

Within these limitations, comparing the data available from these species is a useful first step in exploring suction power across fish. We suggest that when comparing across species, it is most appropriate to compare high performing individuals to each other and lower performing individuals to each other. Within that context, all royal knifefish studied outperform largemouth bass, channel catfish, and bluegill sunfish – Cb01 and Cb03 outperformed the lower performing individuals, just as Cb04 outperformed the highest performing individuals of those species. For the purpose of this discussion, we will compare the highest performing individuals, using them as a proxy for the relative capabilities of each species.

Suction power, intraoral pressure, and buccal expansion

As predicted, royal knifefish are able to produce extremely high magnitudes of suction power (Fig. 7). Royal knifefish generated a mean peak suction power nearly 10 times greater than channel catfish and bluegill sunfish, and 14 times greater than largemouth bass (Fig. 7A; Table S1). When suction power was normalized by body mass, royal knifefish peak mean body mass-specific power was only three times greater than that of bluegill sunfish, yet still 10 times greater than channel catfish and largemouth bass (Fig. 7B). When power is instead normalized to maximum change in buccal volume—the difference between the volume of maximum buccal expansion and initial volume—then royal knifefish are more similar to bluegill sunfish (Fig. 7C). Interestingly, the similarly shaped but distantly related black ghost knifefish (*Apteronotus albifrons*) generated fluid flows during suction feeding that were two to three times greater than largemouth bass or bluegill sunfish (Ortega-Jimenez and Sanford, 2020). While suction power was not measured in this species, it supports our hypothesis that the unusual body shape of knifefishes is linked to fast and forceful suction feeding.

Royal knifefish generated higher suction power by producing both a greater magnitude of subambient intraoral pressure and a greater speed of buccal expansion. Of the four species, the mean peak intraoral pressure was greatest in royal knifefish, followed by bluegill, channel catfish and largemouth bass (Table S1) (Camp et al., 2015; Camp et al., 2018; Camp et al., 2020). Prior studies have not found consistent effects of body size on subambient buccal pressure, so we do not scale pressure here for body size (Carroll et al., 2004; Carroll et al., 2009). However it is unclear how best to compare the rate of volume change among different sized individuals. If we simply compare the raw values across the highest performing individual within each species, the

mean peak rate of buccal volume change was greatest in royal knifefish, more than twice that of largemouth bass and channel catfish, and more than 6.5 times that of bluegill sunfish (Table S1). If we normalize by body mass across the highest performing individual within each species, the mean peak mass-specific rate of buccal volume change was still greater in royal knifefish, more than double that of bluegill sunfish and largemouth bass, and almost five times that of channel catfish. Thus, in comparison to the species previously studied with XROMM, the highest performing royal knifefish individual generated at least three times greater mean power by expanding its buccal cavity two times faster, relative to body mass, and generating at least 1.5 times greater buccal pressure magnitude.

Epaxial muscle shortening and neurocranial elevation

During suction feeding, royal knifefish substantially elevated their neurocranium and cranialmost vertebrae, fully straightening their vertebral column (Fig. 2). Our placement of the body plane near the curve of the vertebral column allowed the neurocranium JCS to capture vertebral column extension along with neurocranial elevation. While the magnitude of rotation was sensitive to location of the body plane, the neurocranium and anterior vertebral column elevated notably and consistently in all three individuals. Compared to the previously studied species, the mean neurocranial elevation in royal knifefish (24.0 ± 0.4 deg) is far greater than in largemouth bass (16.0 ± 0.8 deg), in bluegill sunfish (12.7 ± 1.3 deg), and in channel catfish (-1.6 ± 0.2) (Table S1). Consistent with our predictions, our results indicated that a combination of the initially depressed neurocranium and curved vertebral column increased the range of neurocranial motion used during suction feeding.

In royal knifefish, the mass of the epaxial musculature was approximately 25% of the total body mass and shortened along at least 60-70% of the body length. It accounts for approximately 60% of the muscle mass that shortens to produce suction power (i.e. epaxial, dorsal column, hypaxial, and sternohyoid muscles). Compared to the other species previously studied with XROMM, royal knifefish had a greater proportion of epaxial muscle relative to body mass than bluegill sunfish or channel catfish, but not largemouth bass (Table S1). The hump-like morphology in royal knifefish likely contributes to its relatively large epaxial muscle mass. However, royal knifefish have laterally compressed bodies, thus the greater mediolateral

thickness in largemouth bass likely accounts for the slightly greater proportion of epaxial muscle mass.

In this study and the previous XROMM suction feeding studies, epaxial muscle mass included all of the epaxial musculature dorsal to the vertebral column and about 60-70% along the length of the body, based on the extent of shortening identified with fluoromicrometry, sonomicrometry and electromyography (Camp and Brainerd, 2014; Camp et al., 2018; Camp et al., 2020; Jimenez and Brainerd, 2020; Jimenez et al., 2021). Note that this differs from prior studies, which only included epaxial musculature dorsal to the cleithrum-supracleithrum joint, and which reported lower percentages of epaxial muscle mass in bluegill sunfish and largemouth bass (Carroll, 2004; Carroll and Wainwright, 2009).

Epaxial muscle strain and shortening velocity were higher in royal knifefish than values previously measured in largemouth bass, bluegill sunfish, and channel catfish. The epaxial muscle strain of the highest performing individual in royal knifefish was nearly twice that of largemouth bass and bluegill sunfish (Table S1). Epaxial muscle shortening velocity in royal knifefish was more than double that of largemouth bass and bluegill sunfish (Table S1), shortening at or near the range expected for optimal power output. While the maximum shortening velocity (V_{max}) for royal knifefish epaxials is unknown, V_{max} for largemouth bass has been measured as 11 L_i s^{-1} (Coughlin and Carroll, 2006), so 3-4 L_i s^{-1} is in the range expected for optimal power output. The magnitudes of epaxial strain were correlated with the higher degrees of neurocranial elevation in royal knifefish. Similarly, the increased epaxial shortening velocity in royal knifefish may have caused faster rates of neurocranial elevation and subsequently produced the faster rate of buccal cavity expansion. The combination of these two aspects of epaxial muscle length dynamics, along with high proportions of epaxial muscle mass, likely contributed to the high magnitudes of suction power in royal knifefish.

Hypaxial muscle shortening and cleithral retraction

In the highest performing royal knifefish, Cb04, the cleithrum consistently protracted then retracted as the hypaxial muscle consistently lengthened and then shortened. Cleithral protraction and hypaxial lengthening corresponded to the start of neurocranial elevation and vertebral column extension, which pulled rostro-dorsally on the cleithrum. Because the body plane was placed near the maximum curvature of the vertebral column, cleithrum protraction

628 captures the extension of the vertebral column. The cleithrum does not seem to protract relative
629 to the neurocranium and is likely not reducing buccal volume. Vertebral column extension
630 caused substantial hypaxial lengthening, and thus, even during the period of peak power, the
631 hypaxial muscle was longer than its initial length (-1.5 ± 0.4 % L_i) even as it was shortening near
632 optimal velocity (Fig. 5, Table 1). Compared to the highest performing individual of each
633 species, royal knifefish had twice the hypaxial muscle shortening velocity of largemouth bass
634 and bluegill sunfish, and three times that of channel catfish (Table S1). Because the vertebral
635 column remained partially extended after peak extension, shortening of the hypaxial back to just
636 its initial length still retracted the cleithrum -6.4 ± 0.2 degrees past its initial position.
637 While the ventral muscle markers in Cb01 were implanted ventral to the hypaxial muscle,
638 in the anal fin muscle (Fig. S1), its muscle length traces seemed to align with the cleithral
639 retraction patterns, like the hypaxial length traces of Cb04 (Fig. 5). This suggests that anal fin
640 data may still be reflective of hypaxial strain, but possibly more variable in lower power strikes.
641
642 **Sternohyoid muscle shortening and contributions to suction power**
643 The timing and magnitude of sternohyoid shortening were relatively consistent across all
644 strikes, irrespective of suction power and individual. All individuals had mean magnitudes of
645 peak strain within a similar range of 2.3-3.0 % L_i, but mean peak shortening velocity varied more
646 between individuals, ranging from 4.6 ± 0.2 L_i s^{-1} to 2.3 ± 0.4 L_i s^{-1} (Table 1). The sternohyoid
647 shortened or reached maximum shortening during the period of peak power, which suggests that
648 it actively contributed to buccal cavity expansion. Consistent sternohyoid shortening similarly
649 occurred during buccal cavity expansion in channel catfish, bluegill sunfish, striped surfperch
650 (*Embiotoca lateralis*), and one clariid catfish (Camp et al., 2018; Camp et al., 2020; Lomax et
651 al., 2020; Van Wassenbergh et al., 2007). By contrast, in largemouth bass and several clariid
652 catfishes, the sternohyoid did not shorten (or lengthen) during rapid suction expansion but rather
653 acted as a stiff ligament that transmitted power from hypaxial musculature to produce hyoid
654 depression (Camp and Brainerd, 2014; Van Wassenbergh et al., 2007). Because the sternohyoid
655 did not lengthen in royal knifefish, it inherently transmitted power generated from hypaxial
656 shortening to facilitate hyoid depression and buccal expansion. This suggests that the
657 sternohyoid has a dual function in royal knifefish, both transmitting power from the hypaxial
658 muscle and generating power by shortening during the period of peak power.

The consistent pattern of sternohyoid shortening across all individuals suggests that the sternohyoid muscle may provide a greater proportion of muscle power in low performance strikes. As described in our results, to generate the suction power for the highest recorded strike in Cb04 (161.5 W), the active muscle (epaxial, dorsal column, hypaxial, and sternohyoid) would need to generate 794.1 W kg^{-1}. If the sternohyoid in Cb04 (0.0046 kg) were to operate at this maximum muscle mass-specific power (794.1 W kg^{-1}), then it would be able to generate 3.7 W, which is within the range of the lowest power strikes recorded in Cb01 and Cb03. We estimated that the sternohyoid in Cb01 (0.002 kg) could produce up to 1.6 W of power, which is more than is necessary for suction expansion in the lowest power strike (1.1 W) from Cb01. However, even though the sternohyoid could produce all the power necessary for suction expansion in the lowest power strikes, it is unlikely that it is the sole contributor since the neurocranium elevates and the epaxials shorten to some degree in all strikes (Fig. 5). Instead, it is likely that the sternohyoid makes a greater contribution to generating suction expansion power when epaxial shortening is low and hypaxial muscle shortening is inconsistent, as observed in Cb01 (Fig. 5). We suggest that high power strikes depend on axial muscle shortening (see below), whereas low power strikes likely use the sternohyoid muscle to generate a greater proportion of muscle power.

Muscle mass-specific power

For high performance strikes, royal knifefish depend on the axial musculature shortening at high velocities to produce the neurocranial elevation and buccal expansion that are necessary to generate high magnitudes of suction power. At least 99.3% of the power for the highest power strike from Cb04 must have come from the axial musculature, based on the relative masses of the head and body muscles. If the major cranial muscles in Cb04 (sternohyoid, 4.6 g; levator arcus palatini, 1.64 g; levator operculi, 1.04 g; dilator operculi, 0.024 g) operated at the maximum muscle mass-specific power observed (794.1 W kg^{-1}), the cranial muscles could generate 5.8 W of suction power. For Cb04, 5.8 W is just 0.7% of the maximum suction power and 0.9% of the next three highest power strikes. These results are consistent with the findings of previous studies, which have shown that cranial muscles are only capable of contributing a small proportion of the power necessary for high performance suction feeding and that the axial muscles are the primary source of suction power (Camp and Brainerd 2014; Camp et al., 2015; Camp et al., 2018; Camp et al., 2020).

690 Although we expected that royal knifefish would depend on their axial muscles to
691 generate high power strikes, we didn't expect the axial muscles to operate at exceptionally high
692 muscle mass-specific power in the most powerful strikes. Compared to mean muscle mass-
693 specific power outputs of the highest performing largemouth bass (59.5 ± 9.8 W kg^{-1}), bluegill
694 sunfish (267.0 ± 48.8 W kg^{-1}), and channel catfish (95.7 ± 19.8 W kg^{-1}), Cb04 achieved mean
695 muscle mass-specific power output of 515.0 ± 11.8 W kg^{-1} (Table S1), with a maximum of 794.1
696 W kg^{-1}. This maximum muscle mass-specific power output of nearly 800 W kg^{-1} in Cb04 is near
697 or potentially beyond the expected limits for vertebrates (Altringham et al., 1993; Askew and
698 Marsh, 2001; Curtin et al., 2005), suggesting several possible explanations: 1) we overestimated
699 suction power; 2) we underestimated the longitudinal extent of the axial musculature that is
700 contributing suction power; 3) there is power amplification, in which the muscle shortens before
701 the skeletal elements begin to move, thereby loading serial elastic elements that release their
702 power while the muscle continues to contract as the bones move (Astley and Roberts, 2012).
703 In considering these three possible explanations, we think our suction power estimates
704 are conservative because we measured buccal pressure in just one location close to the front of
705 the buccal cavity, and hydrodynamic modeling has shown that pressure can be even more
706 subambient in the caudal buccal cavity (Van Wassenburgh, 2015). Additionally, when measuring
707 muscle mass to determine muscle mass-specific power estimates, we dissected and included the
708 mass of nearly 75% of the total epaxial and hypaxial length (Fig. S1). Our muscle dissection
709 continued more caudally than our implanted marker set in order to provide a generous muscle
710 mass estimate. Power amplification, as is seen in the epaxial musculature of pipefishes (Van
711 Wassenbergh et al., 2008) is an exciting potential explanation, but our results do not support this
712 hypothesis. If power amplification were to create a catapult-like mechanism, we would expect to
713 see gradual muscle shortening prior to the beginning of the strike to store elastic energy in the
714 muscle and connective tissues (Astley and Roberts, 2012; Van Wassenbergh et al., 2008).
715 However, there was no indication of muscle shortening prior to the beginning of neurocranial
716 elevation nor pectoral girdle retraction (Fig. 5). We conclude that power amplification is unlikely
717 the cause of such high muscle mass-specific muscle power estimates and that Cb04 was able to
718 power suction feeding directly with 600-800 W kg^{-1} of muscle power in its four most powerful
719 suction strikes.
720

Concluding remarks

Compared to the three species previously studied with XROMM, royal knifefish are distinct in the morphology of their postcranial musculoskeletal system and the power they produce for suction feeding. The large and rapid cranial elevation observed of royal knifefish was enabled by the ventrally flexed vertebral column, depressed neurocranium, and a relatively large mass of epaxial musculature. This supports the growing evidence that postcranial morphology is important for understanding suction feeding mechanics, and that these feeding functions have likely shaped the evolution of the axial muscles and skeleton. Royal knifefish used nearly their entire body musculature to generate their most powerful strikes, broadening the morphological and phylogenetic range of suction feeding fish known to power feeding with body muscles. However, the sternohyoid muscle likely contributed a greater proportion of power in the lowest performance strikes, demonstrating that the roles of cranial and axial muscle may vary not only across species, but also among feeding behaviors. Further studies examining the cranial and axial musculoskeletal systems—and their interaction—are needed to understand how the morphology of the whole body shapes the evolution and mechanics of suction feeding.

ACKNOWLEDGEMENTS

We are grateful to Erika Tavares for research administrative support and manuscript edits, to Peter Falkingham and Stephen Gatesy for their assistance in developing the methods for the dynamic digital endocast, to David Baier for the XROMM Maya Tools, and to Jake Parsons, Noah Sims, and Paola Vazquez for their assistance tracking videos.

COMPETING INTERESTS

We declare no competing or financial interests.

FUNDING

This work was supported by the US National Science Foundation [DBI-1612230 to A.M.O., IOS-1655756 to E.L.B. and A.L.C., DBI-1661129 to E.L.B., and DGE-1644760 to E.B.K.], the UK Biotechnology and Biological Sciences Research Council [Fellowship BB/ R011109/1 to A.L.C.], and the Bushnell Research and Education Fund [E.B.K., A.M.O.].

DATA AVAILABILITY

X-ray video, pressure, and CT data and their essential metadata for this publication have been deposited in the XMAPortal (xmaportal.org), in the study "Knifefish Suction Feeding," with the permanent identifier BROWN65, and will be publicly available under CCBY 4.0 upon publication.

REFERENCES

Altringham, J. D., Wardle, C. S. and Smith, C. I. (1993). Myotomal muscle function at different locations in the body of a swimming fish. *J. Exp. Biol.* **182**, 191–206.

Askew, G. N. and Marsh, R. L. (2001). The mechanical power output of the pectoralis muscle of blue-breasted quail (*Coturnix chinensis*): the in vivo length cycle and its implications for muscle performance. *J. Exp. Biol.* **204**, 3587–3600.

Astley, H. C. and Roberts, T. J. (2012). Evidence for a vertebrate catapult: elastic energy storage in the plantaris tendon during frog jumping. *Biol. Lett.* **8**, 386–389. doi:10.1098/rsbl.2011.0982

Astley, H. C., Abbott, E. M., Azizi, E., Marsh, R. L., Roberts, T. J. (2013). Chasing maximal performance: a cautionary tale from the celebrated jumping frogs of Calaveras County. *J. Exp. Biol.*. **216**, 3947-3953. doi:10.1242/jeb.090357.

Betancur-R, R., Wiley, E. O., Arratia, G., Acero, A., Bailly, N., Miya, M., Lecointre, G. and Ortí, G. (2017). Phylogenetic classification of bony fishes. *BMC Evol. Biol.* **17**, 1–40. doi:10.1186/s12862-017-0958-3

Brainerd, E. L., Baier, D. B., Gatesy, S. M., Hedrick, T. L., Metzger, K. A., Gilbert, S. L. and Crisco, J. J. (2010). X-ray reconstruction of moving morphology (XROMM): precision, accuracy and applications in comparative biomechanics research. *J. Exp. Zool. Part A Ecol. Genet. Physiol.* **313A**, 262–279. doi:10.1002/jez.589

Brainerd, E. L., Blob, R. W., Hedrick, T. L., Creamer, A. T. and Müller, U. K. (2017). Data management rubric for video data in organismal biology. *Integr. Comp. Biol.* **57**, 33–47. doi:10.1093/icb/icx060

Camp, A. L. and Brainerd, E. L. (2014). Role of axial muscles in powering mouth expansion during suction feeding in largemouth bass (*Micropterus salmoides*). *J. Exp. Biol.* **217**, 1333–1345. doi:10.1242/jeb.095810

Camp, A. L., Roberts, T. J. and Brainerd, E. L. (2015). Swimming muscles power suction feeding in largemouth bass. *Proc. Natl. Acad. Sci.* **112**, 8690–8695. doi:10.1073/pnas.1508055112

Camp, A. L., Astley, H. C., Horner, A. M., Roberts, T. J. and Brainerd, E. L. (2016). Fluoromicrometry: A method for measuring muscle length dynamics with biplanar videofluoroscopy. *J. Exp. Zool.* **325A**, 399–408. doi:10.1002/jez.2031

Camp, A. L., Roberts, T. J. and Brainerd, E. L. (2018). Bluegill sunfish use high power outputs from axial muscles to generate powerful suction-feeding strikes. *J. Exp. Biol.* **221**. doi:10.1242/jeb.178160

Camp, A. L., Olsen, A. M., Patricia Hernandez, L. and Brainerd, E. L. (2020). Fishes can use axial muscles as anchors or motors for powerful suction feeding. *J. Exp. Biol.* **223**. doi:10.1242/jeb.225649

Carroll, A. M. (2004). Muscle activation and strain during suction feeding in the largemouth bass *Micropterus salmoides*. *J. Exp. Biol.* **207**, 983–991. doi:10.1242/jeb.00862

Carroll, A. M. and Wainwright, P. C. (2009). Energetic limitations on suction feeding performance in centrarchid fishes. *J. Exp. Biol.* **212**, 3241–3251. doi:10.1242/jeb.033092

Carroll, A. M., Wainwright, P. C., Huskey, S. H., Collar, D. C. and Turingan, R. G. (2004). Morphology predicts suction feeding performance in centrarchid fishes. *J. Exp. Biol.* **207**, 3873–3881. doi:10.1242/jeb.01227

Carroll, A. M., Ambrose, A. M., Anderson, T. A. and Coughlin, D. J. (2009). Feeding muscles scale differently from swimming muscles in sunfish (Centrarchidae). *Biol. Lett.* **5**, 274–277. doi:10.1098/rsbl.2008.0647

Collar, D. C. and Wainwright, P. C. (2006). Discordance between morphological and mechanical diversity in the feeding mechanism of centrarchid fishes. *Evolution.* **60**, 2575–2584. doi:10.1111/j.0014-3820.2006.tb01891.x

Coombs, S. and Popper, A. N. (1982). Structure and function of the auditory system in the clown knifefish, *Notopterus chitala*. *J. Exp. Biol.* **97**, 225–239. doi:10.1242/jeb.97.1.225

Coughlin, D. J. and Carroll, A. M. (2006). In vitro estimates of power output by epaxial muscle during feeding in largemouth bass. *Comp. Biochem. Physiol. Part A Mol. Integr. Physiol.* **145**, 533–539. doi:10.1016/j.cbpa.2006.08.026

Curtin, N. A., Woledge, R. C. and Aerts, P. (2005). Muscle directly meets the vast power demands in agile lizards. *Proc. R. Soc. B* **272**, 581–584. doi:10.1098/rspb.2004.2982

Gidmark, N. J., Staab, K. L., Brainerd, E. L. and Hernandez, L. P. (2012). Flexibility in starting posture drives flexibility in kinematic behavior of the kinethmoid-mediated

premaxillary protrusion mechanism in a cyprinid fish, *Cyprinus carpio*. *J. Exp. Biol.* **215**, 2262–2272. doi:10.1242/jeb.070516

Jimenez, Y. E. and Brainerd, E. L. (2020). Dual function of epaxial musculature for swimming and suction feeding in largemouth bass. *Proc. R. Soc. B* **287**. doi:10.1098/rspb.2019.2631

Jimenez, Y. E. and Brainerd, E. L. In press. Motor control in the epaxial musculature of bluegill sunfish in feeding and locomotion. *J. Exp. Biol.*

Jimenez, Y. E., Camp, A. L., Grindall, J. D. and Brainerd, E. L. (2018). Axial morphology and 3D neurocranial kinematics in suction-feeding fishes. *Biol. Open* **7**. doi:10.1242/bio.036335

Jimenez, Y. E., Marsh, R. L. and Brainerd, E. L. (2021). A biomechanical paradox in fish: swimming and suction feeding produce orthogonal strain gradients in the axial musculature. *Sci. Rep.* **11**, 1–9. doi:10.1038/s41598-021-88828-x

Knörlein, B. J., Baier, D. B., Gatesy, S. M., Laurence-Chasen, J. D. and Brainerd, E. L. (2016). Validation of XMALab software for marker-based XROMM. *J. Exp. Biol.* **219**, 3701–3711. doi:10.1242/jeb.145383

Liem, K. F. (1967). Functional morphology of the head of the anabantoid teleost fish *Helostoma temmincki*. *J. Morphol.* **121**, 135–157. doi:10.1002/jmor.1051210204

Lomax, J. J., Martinson, T. F., Jimenez, Y. E. and Brainerd, E. L. (2020). Bifunctional role of the sternohyoideus muscle during suction feeding in striped surfperch, *Embiotoca lateralis*. *Integr. Org. Biol.* **2**. doi:10.1093/iob/obaa021

Muller, M., Osse, J. W. M. and Verhagen, J. H. G. (1982). A quantitative hydrodynamical model of suction feeding in fish. *J. Theor. Biol.* **95**, 49–79. doi:10.1016/0022-5193(82)90287-9

Norton, S. F. and Brainerd, E. L. (1993). Convergence in the feeding mechanics of ecomorphologically similar species in the centrarchidae and cichlidae. *J. Exp. Biol.* **29**, 11–29. doi:10.1242/jeb.176.1.11

Olsen, A. M., Hernández, L. P., Camp, A. L., Brainerd, E. L., Patricia Hernández, L., Camp, A. L. and Brainerd, E. L. (2019). Channel catfish use higher coordination to capture prey than to swallow. *Proc. R. Soc. B* **286**. doi:10.1098/rspb.2019.0507

Ortega-Jimenez, V. M. and Sanford, C. P. J. (2020). Knifefish's suction makes water boil. *Sci. Rep.* **10**. doi:10.1038/s41598-020-75788-x

Osse, J. W. M. (1969). Functional morphology of the head of the perch (*Perca Fluviatilis L.*): an electromyographic study. *Netherlands J. Zool.* **19**, 289–392. doi:10.1163/002829669X00134

Sanford, C. P. J. and Lauder, G. V. (1989). Functional morphology of the "tongue-bite" in the osteoglossomorph fish *Notopterus*. *J. Morphol.* **202**, 379–408. doi:10.1002/jmor.1052020307

Tegge, S., Hall, J. and Huskey, S. (2020). Spatial and temporal changes in buccal pressure during prey-capture in the trumpetfish (*Aulostomus maculatus*). *Zoomorphology* **139**, 85–95. doi:10.1007/s00435-019-00470-4

Van Wassenbergh, S. (2015). A solution strategy to include the opening of the opercular slits in moving-mesh CFD models of suction feeding. *Integr. Comp. Biol.* **55**, 62–73. doi:10.1093/icb/icv031

Van Wassenbergh, S., Aerts, P. and Herrel, A. (2005). Scaling of suction-feeding kinematics and dynamics in the African catfish, *Clarias gariepinus*. *J. Exp. Biol.* **208**, 2103–2114. doi:10.1242/jeb.01603

Van Wassenbergh, S., Aerts, P. and Herrel, A. (2006). Scaling of suction feeding performance in the catfish *Clarias gariepinus*. *Physiol. Biochem. Zool.* **79**, 43–56. doi:10.1086/498188

Van Wassenbergh, S., Herrel, A., Adriaens, D. and Aerts, P. (2007). Interspecific variation in sternohyoideus muscle morphology in clariid catfishes: functional implications for suction feeding. *J. Morphol.* **268**, 268–242. doi:10.1002/jmor.10510

Van Wassenbergh, S., Strother, J. A., Flammang, B. E., Ferry-Graham, L. A. and Aerts, P. (2008). Extremely fast prey capture in pipefish is powered by elastic recoil. *J. R. Soc. Interface* **5**, 285–296. doi:10.1098/rsif.2007.1124

Van Wassenbergh, S., Day, S. W., Hernández, L. P., Higham, T. E. and Skorczewski, T. (2015). Suction power output and the inertial cost of rotating the neurocranium to generate suction in fish. *J. Theor. Biol.* **372**, 159–167. doi:10.1016/j.jtbi.2015.03.001

880 **TABLES**

881 **Table 1.** Mean (± s.e.m) measurements of peak pressure, change in buccal volume, power, total
882 body mass, bilateral axial and sternohyoid muscle shortening for each individual during peak
883 suction expansion power, and peak muscle power.

884

Variable	Cb01 (N = 6)	Cb03 (N = 6)	Cb04 (N = 10)
Peak pressure, kPa	-7.8 ± 0.8	* -14.9 ± 1.7	-43.7 ± 1.1
Peak change in buccal volume, cm^3	23.4 ± 0.4	* 15.9 ± 0.4	54.2 ± 0.2
Peak rate of volume change, $cm^3\ s^{-1}$	835 ± 51	* 829 ± 67	2518 ± 40
Peak power, W	6.4 ± 0.8	* 14.6 ± 2.1	104.8 ± 3.4
Total body mass, g	217	170	480
Epaxial			
▲ Muscle mass, g	52.7	** 44.1	125.2
Initial muscle length, mm	115.1± 0.3	109.4 ± 0.2	103.4 ± 0.07
Peak muscle strain, %	3.5 ± 0.2	7.6 ± 0.7	7.9 ± 0.2
Peak muscle velocity, $L_i\ s^{-1}$	2.0 ± 0.2	3.2 ± 0.5	4.1± 0.1
Hypaxial			
Muscle mass, g	27.5	** 25.5	73.7
Initial muscle length, mm	100.4 ± 1.2	*** ____	65.3 ± 0.2
Peak muscle strain, %	2.7 ± 1.3	*** ____	-1.5 ± 0.4
Peak muscle velocity, $L_i\ s^{-1}$	1.9 ± 0.4	*** ____	3.8 ± 0.1
Sternohyoid			
Muscle mass, g	2.0	** 1.5	4.6
Initial muscle length, mm	21.2 ± 0.03	9.3 ± 0.02	15.3 ± 0.003
Peak muscle strain, %	3.0 ± 0.4	2.3 ± 0.3	2.6 ± 0.1
Peak muscle velocity, $L_i\ s^{-1}$	2.8 ± 0.3	2.3 ± 0.4	4.6 ± 0.2
Peak muscle mass-specific power, W kg^{-1}	77.9 ± 9.7	* 205.3 ± 29.5	515.0 ± 16.7

Mean ± s.e.m are listed for every variable except for mass. Bilateral muscle mass is listed. Positive values for peak muscle strain (% L_i) and peak muscle velocity ($L_i\ s^{-1}$) represent shortening during period of peak power.

* Pressure, volume, and power values for Cb03 were measured for N = 7

** Bilateral muscle mass was estimated for Cb03 because individual was not available for muscle dissection

*** Hypaxial values are not recorded for Cb03 because shortening was only measured over the dorsal subregion of this individual

▲ Dorsal column muscle mass is included in the total epaxial muscle masses

885

886 **FIGURES**

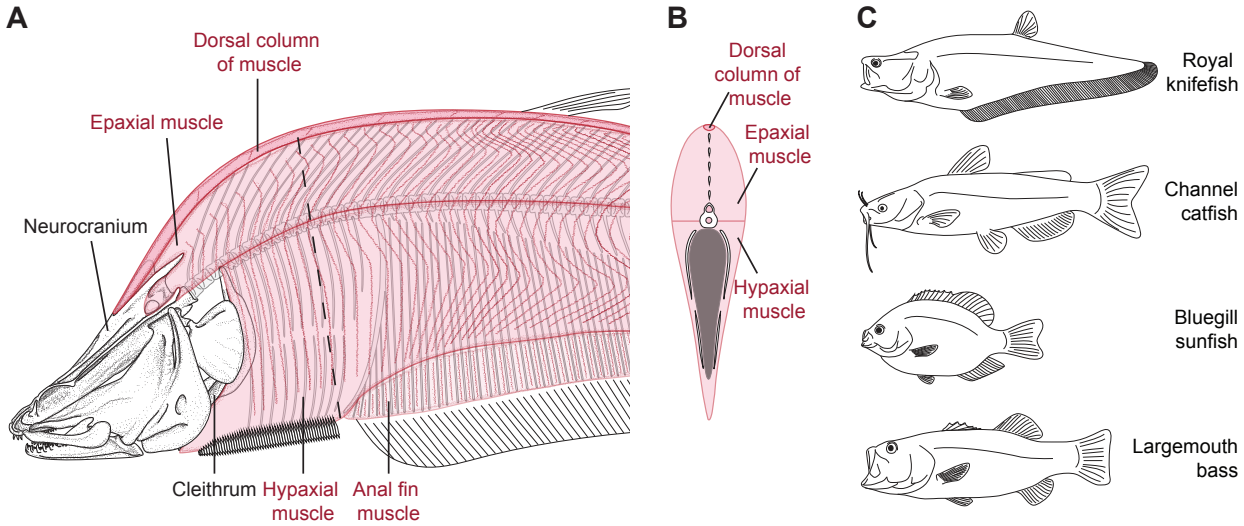

887

888 Fig. 1. Body shape and anatomy of the axial musculature and skeleton in royal knifefish, *Chitala*
889 *blanci*, compared with the body shapes of three other species for which suction power has been
890 measured. (A) Lateral view of the neurocranium, cleithrum, and left-side bones of the cranium in
891 *C. blanci*. Dashed line indicates the approximate location of the cross-section shown in (B). (B)
892 Transverse cross-section of *C. blanci*, illustrating its inverted teardrop shape. (C) Whole-body
893 shape comparison of *C. blanci* to other previously studied suction power species: channel catfish
894 (*Ictalurus punctatus*), bluegill sunfish (*Lepomis macrochirus*), and largemouth bass (*Micropterus*
895 *salmoides*). Fishes are shown with expanded mouths.

896

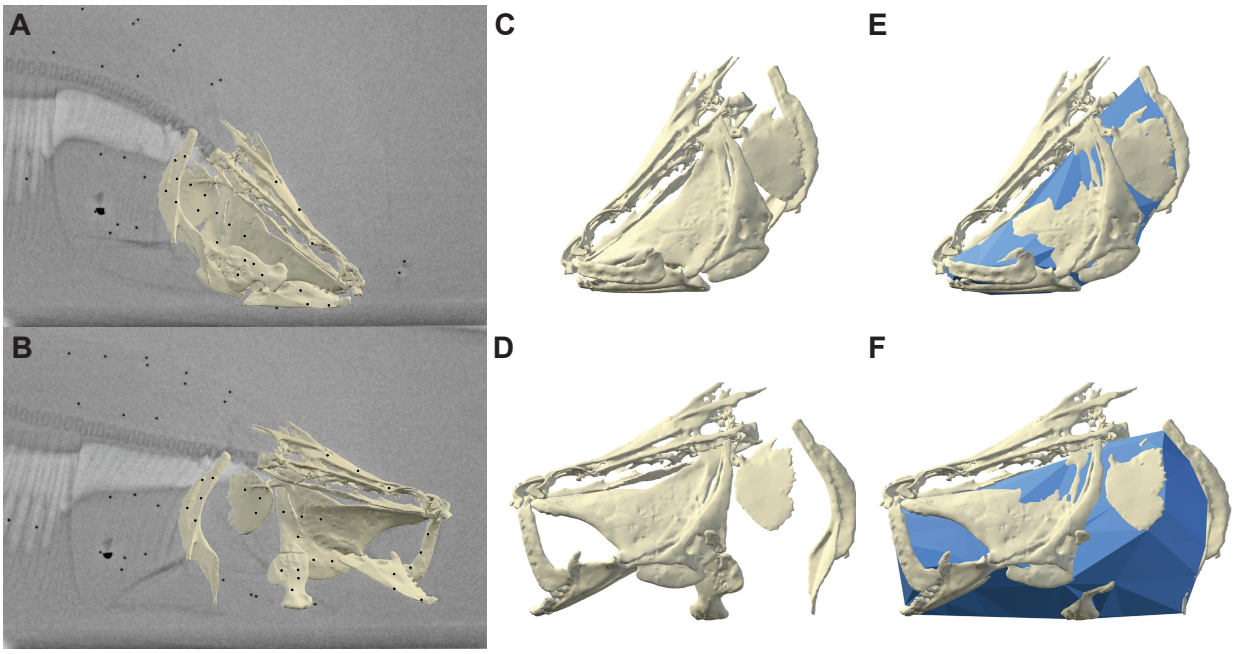

Fig. 2. Sample XROMM animation and measurement of buccal cavity volume before and during suction expansion. Animated bone models before suction expansion (A,C,E) and during suction expansion (B,D,F). (A,B) Right lateral view of X-ray image with animated neurocranium, left cleithrum, and left-side bone meshes. Surgically implanted bone marker sets and intramuscular (epaxial, hypaxial, dorsal column, and sternohyoid) marker sets are visible. (C,D) Left lateral view of animated bone models and (E,F) animated dynamic endocast of buccal cavity volume.

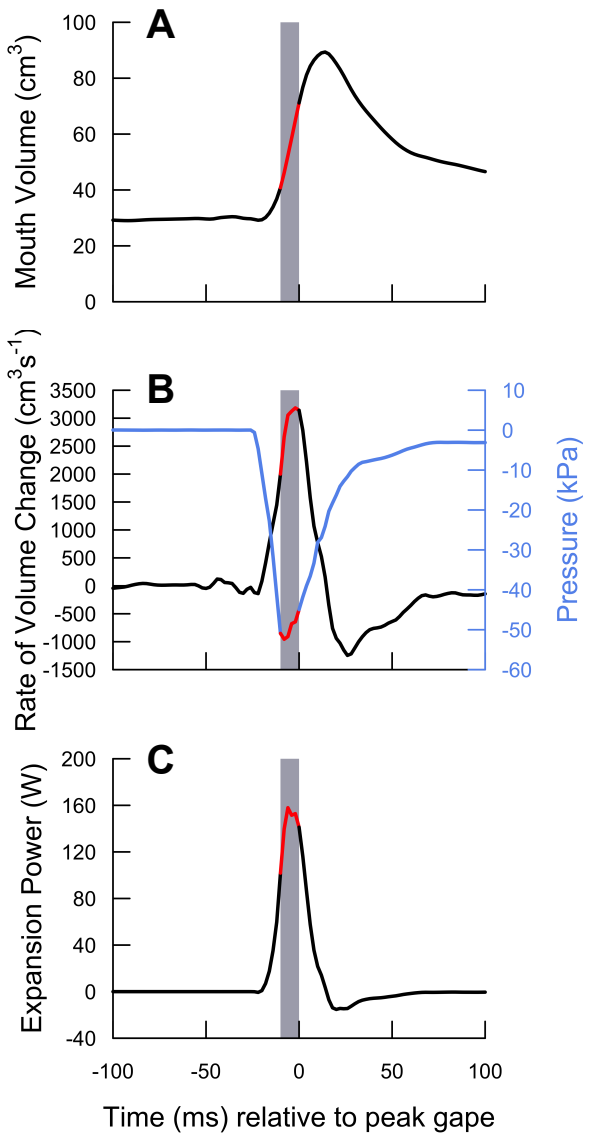

Fig. 3. Buccal volume, intraoral pressure, and suction expansion power in the highest power strike. (A) Buccal volume, calculated using dynamic endocast. (B) Rate of buccal volume change (left axis) and intraoral pressure relative to ambient pressure (right axis). (C) Suction expansion power was calculated as the product of intraoral pressure and rate of buccal volume change at each time point. Peak expansion power (within 25% of maximum) is indicated by the shaded region with the corresponding values highlighted in red.

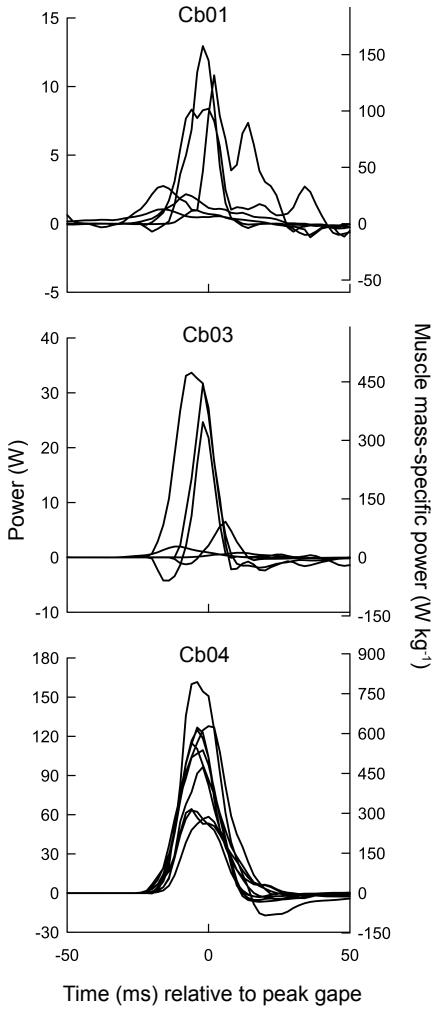

Fig. 4. Estimated suction expansion power (W) and muscle mass-specific power (W kg-1) in three royal knifefish. Absolute suction expansion power is plotted relative to peak gape for each strike in each individual. The left y-axis represents absolute suction expansion power and the right y-axis shows muscle mass-specific power, which divides suction expansion power by the total muscle mass of the epaxial and hypaxial shortening regions and the sternohyoid.

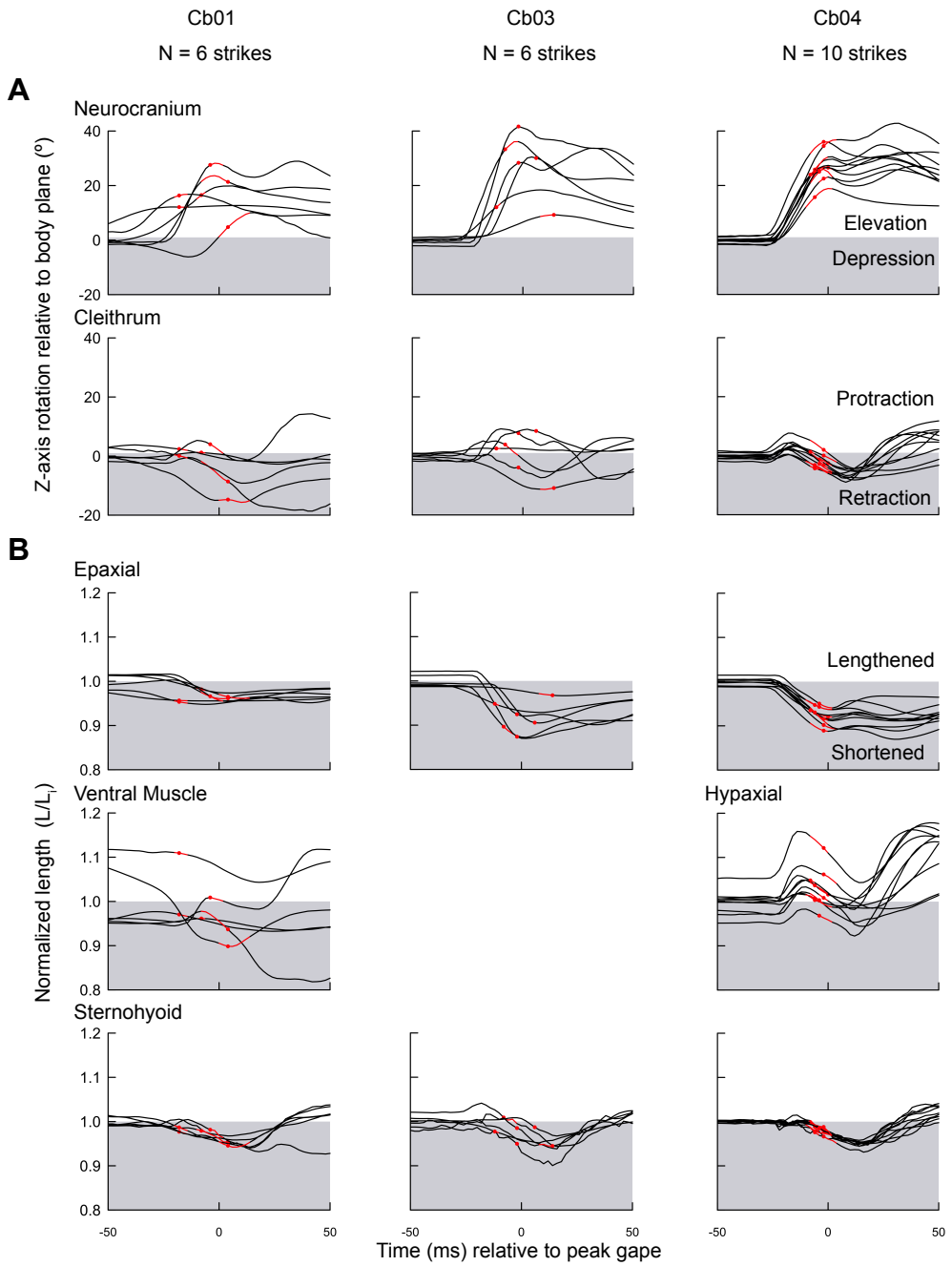

Fig. 5. Neurocranium and cleithrum rotations relative to the body plane and muscle length changes during buccal expansion in royal knifefish. Data from each individual is separated into three columns. (A) Z-axis rotation (relative to initial values) was measured for the neurocranium (row 1) and left cleithrum (row 2) relative to the body plane. Positive values represent elevation or protraction (white region), while negative values represent depression or retraction (shaded region). (B) For each muscle (bottom three rows), muscle length was normalized by the mean initial length (L_i) of each muscle and values below 1 (shaded region) represent shortened muscle,

while those greater than 1 (white region) represent lengthened muscle relative to L_i. The curves (black lines) are aligned by the timing of peak gape. The muscle lengths and z-axis rotations occurring during peak suction expansion power (within 25% of maximum) are highlighted in red (red dot indicates time of peak power).

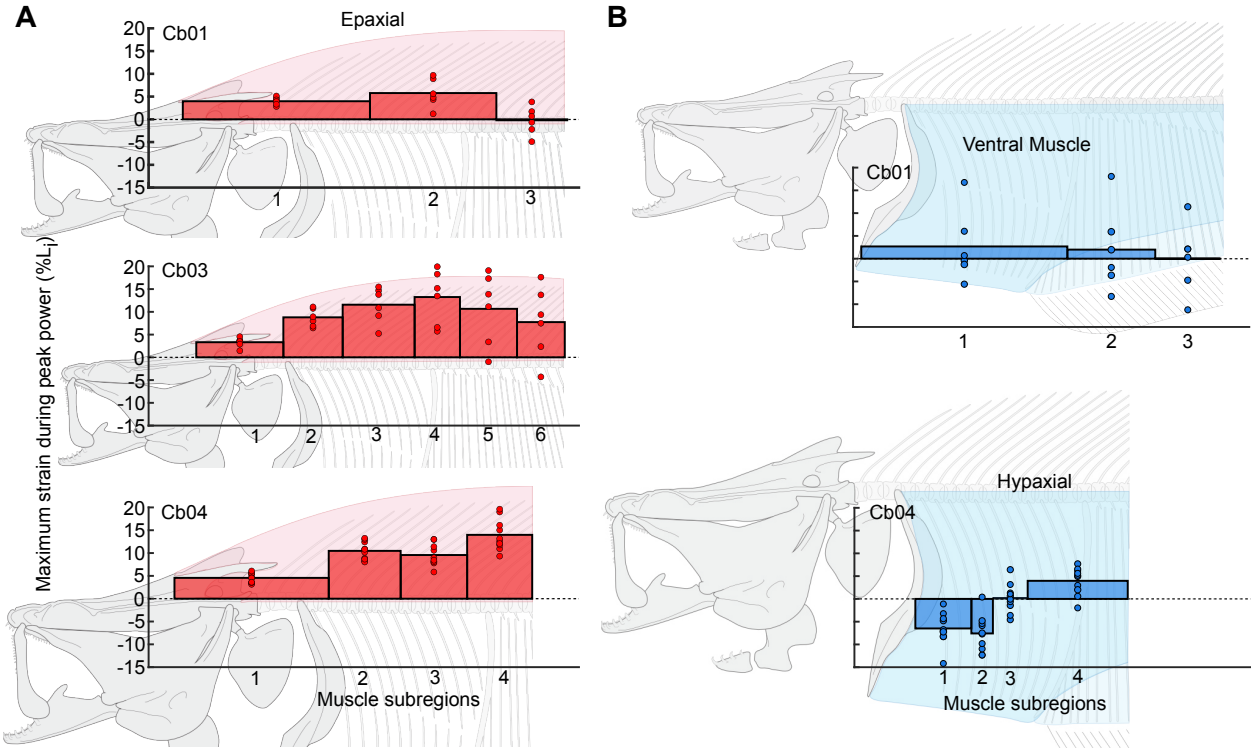

933

934 Fig. 6. Maximum epaxial and hypaxial muscle strain along the body. (A) Dorsal epaxial strain
935 and (B) ventral (anal fin) muscle/hypaxial strain were calculated as percent change in length
936 relative to the mean initial length (L_i) in subregions along the cranial half of the body length.
937 Maximum strain during peak expansion for each strike (red or blue circles) and mean strain (red
938 or blue bars) across all strikes are shown for each subregion with positive strain representing
939 muscle shortening. The width of the bar reflects the craniocaudal length of each muscle
940 subregion. Note that Cb03 did not have a ventral muscle marker set, so strain was not calculated.
941

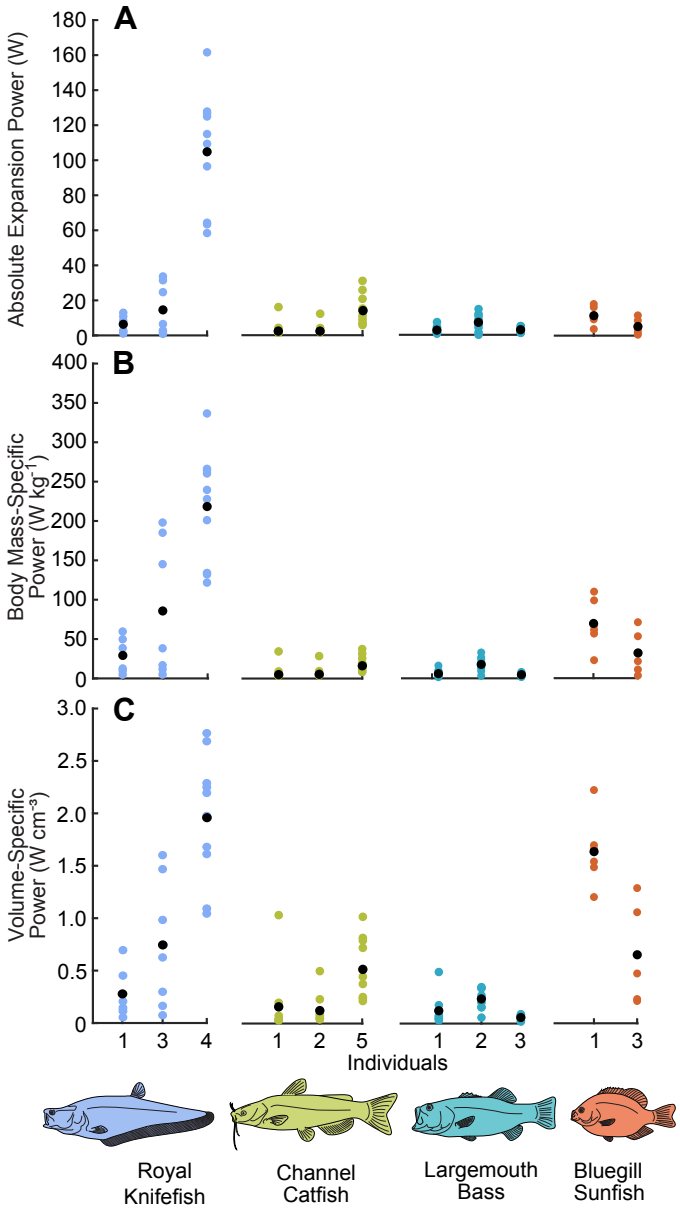

Fig. 7. Comparison of estimated expansion power of royal knifefish to three other species. Data are shown for royal knifefish (n = 23 strikes, from this study), channel catfish (n = 24 strikes, data from Camp et al., 2020), largemouth bass (n = 29 strikes, data from Camp et al., 2015), and bluegill sunfish (n = 11 strikes, data from Camp et al., 2018). Power per strike (colored circles) and average power across all strikes from each individual (black circles) are shown. For all species, estimated suction expansion power was calculated as (A) the absolute magnitude of maximum expansion power, (B) maximum expansion power relative to the total body mass of the individual, and (C) maximum expansion power relative to the maximum change in buccal volume for each strike.